0026-895X/97/010109-10$3.00/0

MOLECULAR PHARMACOLOGY, **51:**109–118 (1997).

Characterization of Recombinant Human $P2X_4$ Receptor Reveals Pharmacological Differences to the Rat Homologue

MIGUEL GARCIA-GUZMAN, FLORENTINA SOTO, JUAN MANUEL GOMEZ-HERNANDEZ, PER-ERIC LUND, and WALTER STÜHMER

Department of Molecular Biology of Neuronal Signals, Max-Planck Institute for Experimental Medicine, Hermann-Rein-Str. 3, D-37075 Göttingen, Germany

Received July 29, 1996; Accepted September 24, 1996

SUMMARY

We isolated a cDNA from human brain encoding a purinergic receptor that shows a high degree of homology to the rat $P2X_4$ receptor (87% identity). By fluorescence *in situ* hybridization, the human $P2X_4$ gene has been mapped to region q24.32 of chromosome 12. Tissue distribution analysis of human $P2X_4$ transcripts demonstrates a broad expression pattern in that the mRNA was detected not only in brain but also in all tissues tested. Heterologous expression of the human $P2X_4$ receptor in *Xenopus laevis* oocytes and human embryonic kidney 293 cells evoked an ATP-activated channel. Simultaneous whole-cell current and Fura-2 fluorescence measurements in human embryonic kidney 293 cells transfected with human $P2X_4$ cDNA allowed us to determine the fraction of the current carried by Ca^{2+}; this was ~8%, demonstrating a high Ca^{2+} permeability. Low extracellular Zn^{2+} concentrations (5–10 μM) increase the apparent gating efficiency of human $P2X_4$ by ATP without affecting the maximal response. However, raising the concentration of the divalent cation (>100 μM) inhibits the ATP-evoked current in a non-voltage-dependent manner. The human $P2X_4$ receptor displays a very similar agonist potency profile to that of rat $P2X_4$ (ATP $\gg$ 2-methylthio-ATP $\geq$ CTP $>$ α,β-methylene-ATP $>$ dATP) but has a notably higher sensitivity for the antagonists suramin, pyridoxal-phosphate-6-azophenyl-2′,4′-disulfonic acid, and bromphenol blue. Chimeric constructs between human and rat isoforms as well as single-point mutations were engineered to map the regions responsible for the different sensitivity to suramin and pyridoxal-phosphate-6-azophenyl-2′,4′-disulfonic acid.

The binding of ATP to P2-purinergic receptors exerts widespread biological responses in different tissues, where it regulates central and peripheral nervous system signaling, blood vessel contractility, and endocrine secretion among other functions (for reviews, see Refs. 1–3). In 1985, based on the order of potency of different nucleotide analogs, these receptors were initially classified by Burnstock and Kennedy into P2X and P2Y subgroups (4). According to the signal transduction mechanism the P2X receptors constitute a subclass of ligand-gated channels while the P2Y subgroup represent metabotropic receptors.

The activation of P2X receptors leads to the opening, in the millisecond range, of nonselective cation channels permeable to Na^+ and K^+. Certain P2X receptors are also permeable to Ca^{2+} (5, 6). Pharmacologically, the agonist potency of α,β-meATP and the antagonist effects of suramin and PPADS have been useful tools with which to define native P2X-mediated responses. In different cell types, the P2X receptors seem to have similar but not identical ligand binding selectivities (7), clearly suggesting the existence of multiple subclasses.

Recently, molecular biological studies have confirmed P2X diversity at the protein level. Seven isoforms have been cloned from different rat tissues, $rP2X_{1\text{-}7}$ (Ref. 8 and references therein; 9, 10), and one isoform has been cloned from human bladder, $hP2X_1$ (11). The rP2X subtypes share an overall amino acid identity of only 35–50%, but the conservation of the main structural features (two putative transmembrane segments flanking a putatively extracellular loop containing 10 cysteine residues) suggest a common three-dimensional structure (8). The different isoforms, except $rP2X_3$ (12), display a widespread mRNA distribution (9, 10, 13, 14). It is remarkable that $rP2X_4$ transcripts are detected in all the tissues analyzed, including central nervous system neurons (15).

In heterologous expression systems, the cloned P2X subunits assemble into functional homomeric receptors with unique pharmacological and kinetic properties. Despite some

P.E.L. was supported by a Human Frontiers Science Program Fellowship. M. G.-G. and F. S. contributed equally to this work.

ABBREVIATIONS: α,β-meATP, α,β-methylene-ATP; rP2X, rat P2X; hP2X, human P2X; β,γ-meATP, β,γ-methylene-ATP; PPADS, pyridoxal-phosphate-6-azophenyl-2′,4′-disulfonic acid; PHA, phytohemagglutinin; 2MeSATP, 2-methylthio-ATP; PCR, polymerase chain reaction; RT, reverse transcription; HEPES, 4-(2-hydroxyethyl)-1-piperazineethanesulfonic acid; HEK, human embryonic kidney; bp, base pairs; FISH, fluorescence *in situ* hybridization; $[Zn^{2+}]_o$, extracellular Zn^{2+} concentration.

variation in ATP sensitivity, the main pharmacological distinction between the P2X isoforms is their relative sensitivities to the agonists α,β-meATP and β,γ-meATP and the antagonists suramin and PPADS (16). Currents evoked by ATP in cells expressing the $rP2X_4$ (15) and $rP2X_6$ (16) receptors are weakly affected by suramin and PPADS. On the other hand, the same antagonists completely block the $rP2X_1$ (12), $hP2X_1$ (17), $rP2X_2$ (17), $rP2X_3$ (12), and $rP2X_5$ (9) receptors (IC_{50} = 1–5 μM). Structural studies have demonstrated that the irreversible block of PPADS requires a lysine residue at position 249 (of $rP2X_4$) (16, 18), but no structural data have been described for the suramin binding pocket.

We report the cloning and functional characterization of the $P2X_4$ isoform from human brain ($hP2X_4$). In addition, we describe significant pharmacological differences concerning the antagonist potencies between the human and rat isoforms and delimit the structural requirements conferring the different phenotypes.

Materials and Methods

Drugs. ATP (disodium salt), CTP (sodium salt), UTP (sodium salt), α,β-meATP, (lithium salt), D-β,γ-meATP (sodium salt), cibacron blue 3GA, bromphenol blue, basilen blue, (+)-tubocurarine (chloride), dATP (sodium salt), and AMP (sodium salt) were obtained from Sigma Chemical (St. Louis, MO). GTP (disodium salt) was purchased from Fluka Chemical (Ronkonkoma, NY). ADP (free acid) was obtained from Boehringer-Mannheim Biochemicals (Indianapolis, IN). PPADS (tetrasodium salt) and 2MeSATP (tetrasodium salt) were obtained from Research Biochemicals (Natick, MA). Suramin was purchased from Calbiochem (San Diego, CA). Fura-2 was obtained from Molecular Probes (Eugene, OR).

cDNA synthesis and PCR amplification. Poly(A)$^+$ RNA was purified from human brain total RNA (75 μg) (Clontech, Palo Alto, CA) using oligo(dT)$_{25}$ magnetic beads (Dynal, Lake Success, NY) according to the manufacturer's recommendations. For the first-strand cDNA synthesis (19), the resulting mRNA was divided in two aliquots, primed separately with oligo(dT)$_{12-18}$ or random hexamers, and extended using the SuperScript Plus Reverse Transcriptase (GIBCO, Grand Island, NY). After enzyme inactivation, the differently primed cDNAs were diluted with 1 volume of H_2O and mixed for PCR analysis.

Degenerate oligonucleotides targeted to conserved P2X amino acid sequences were used for PCR (PCR Master Kit, Boehringer-Mannheim) analysis of 1 μl of cDNA as previously described (15). The PCR products were separated in an agarose gel, purified, cloned, and sequenced using the dideoxynucleotide chain termination method (20).

Library screening. A human brain cDNA library (Clontech) was screened by lifting 1×10^6 phages to nylon membranes (Duralon-UV; Stratagene, La Jolla, CA) as described previously (21). The $hP2X_4$ PCR fragment isolated from human brain cDNA (~750 bp) was labeled with [α-^{32}P]dCTP (specific activity, 3000 Ci/mmol) by random priming with the Redyprime kit (Amersham, Arlington Heights, IL). Hybridization of probes (5×10^5 cpm/ml) with the filters and washing was performed under the conditions previously described (15). The λ phages found to hybridize to the probe were subsequently plaque purified, subcloned into pBluescript SK(II) (Stratagene), and sequenced (see below). Other standard nucleic acid manipulations were performed using conventional protocols (21).

Nested deletions were made by the DNase I method (22), and the sequence from both strands was determined by the dideoxynucleotide chain termination method (20).[1]

RT-PCR. First-strand cDNA synthesis reactions were performed using total RNA from various adult human tissues (Clontech) as indicated above. The PCR reactions were performed in 50-μl final volumes containing 1 μl of cDNA, 0.5 μM each of pairs of $hP2X_4$-specific primers, 200 μM dNTPs, 2.5 units of *Taq* DNA polymerase, and 1× *Taq* DNA polymerase reaction buffer (Promega, Madison, WI). The PCR thermal profile was 5 min at 94° and 30 cycles of 40 sec at 94°, 40 sec at 58°, and 60 sec at 72°. The $hP2X_4$ primers were (forward, located within the protein coding sequence) 5′-CACCCACAGCAACGGAGTCT-3′ and (reverse, located within the 3′ untranslated region) 5′-TTTGATGGGGCTGTGGAGAG-3′. The PCR products were separated in an agarose gel and visualized with ethidium bromide staining. The specificity of the amplification bands was confirmed by determination of the nucleotide sequence. As negative controls, 0.5 μg of human genomic DNA and a sample with no target cDNA (H_2O) were subjected to the same amplification protocol.

FISH and detection. Cell preparation and FISH were performed as previously described (23). Briefly, lymphocytes isolated from human blood were cultured in α-minimal essential medium supplemented with 10% fetal calf serum and PHA at 37° for 68–72 hr. The cells were washed three times with serum-free medium to release the block and recultured at 37° for 6 hr in α-minimum essential medium with thymidine (2.5 μg/ml; Sigma). The cells were then harvested, and slides were made by using standard procedures involving hypotonic treatment, fixation, and air drying.

A full-length $hP2X_4$ probe (1.7 kb) was biotinylated with dATP using the BRL BioNick labeling kit (15° for 1 hr) (GIBCO BRL, Baltimore, MD). Briefly, slides were backed at 55° for 1 hr. After RNase treatment, the slides were denatured in 70% formamide in 2× standard saline citrate (1× = 150 mM NaCl, 15 mM sodium citrate, pH 7.2) for 2 min at 70° followed by ethanol dehydration. Probes were denatured at 75° for 5 min in a hybridization mix consisting of 50% formamide and 10% dextran sulfate and loaded onto the denatured chromosomal slides. After overnight hybridization, slides were washed, detected, and amplified. FISH signals and the DAPI banding pattern were recorded separately photographically, and the assignment of the FISH mapping data with chromosomal bands was achieved by superimposing FISH signals onto DAPI banded chromosomes (24).

DNA mutagenesis and RNA synthesis. Chimeric DNA constructs were engineered by using common endonuclease restriction enzymes for both species. Single-point mutations were made using PCR approaches as described previously (25). The nucleotide sequence of the amplified DNA fragments was determined to ensure the absence of random mutations.

The full-length clone $hP2X_4$ and the chimeric and point mutations constructs were inserted into the pSGEM vector (15). Plasmid DNA was purified using the Wizard DNA system (Promega). Capped cRNA was transcribed *in vitro* (26) with T7 RNA polymerase (Promega) in the presence of the cap analog $m^7G(5')ppp(5')G$ (Boehringer-Mannheim), using 5 μg of *Nhe*I-linearized DNA. The cRNA was examined on ethidium bromide-stained denaturing agarose gels to ensure the presence of a single, nondegraded band of the expected size. The final cRNA concentration was ~0.25 mg/ml, as estimated visually by comparing it with the known amount of molecular weight standards, and was used directly for *Xenopus laevis* oocyte injection.

Electrophysiological characterization. Oocyte isolation and handling were performed using standard techniques (27). Two electrode voltage-clamp recordings were performed 1–10 days after cRNA injection. Unless otherwise indicated, the standard Mg^{2+} solution used to superfuse the oocytes contained 115 mM NaCl, 2.8 mM KCl, 1.8 mM $MgCl_2$, and 10 mM HEPES, pH 7.2. This Ca^{2+}-free solution was used to avoid activation of Ca^{2+}-dependent Cl^- channels. The drugs were prepared as concentrated stocks in 100 mM HEPES, pH 7.2, and stored at −20° until use. Solutions at the desired concentration were freshly made from the frozen stocks and used for ≤2 hr. The small volume of the bath in the recording chamber (<100 μl) and the high rate of perfusion (7–10 ml/min)

[1] The nucleotide sequence of $hP2X_4$ cDNA has been submitted to GeneBank with accession number Y07684.

allowed a rapid exchange of solutions. The recovery of the current was complete after <2 min of wash-out, even at the highest concentrations of ATP used. Nevertheless, we allowed a 3-min wash-out period between two successive recordings. Unless otherwise indicated, antagonists and Zn^{2+} were coapplied with ATP during perfusion with the standard Mg^{2+} solution. PPADS was preincubated for 4–8 min before ATP stimulation.

Voltage and current electrodes were filled with 2 M KCl solution and had resistances of 0.5–1.5 MΩ. All experiments were performed at room temperature (18–22°). Currents were recorded using a Turbo TEC-10CD amplifier (NPI electronics, Lambrecht, Germany) and Pulse software (HEKA, Tamm, Germany) and filtered at 20 Hz. Voltage ramps (−100 mV to +70 mV in 150 msec) were applied when the current had reached steady state and filtered at 1 kHz. The final values were corrected for leak currents that were obtained performing the same voltage ramps under the appropriate solutions, immediately before ATP stimulation.

For all data, error bars represent standard deviation.

Fura-2-based measurements of Ca^{2+} influx. Permanent transfection of HEK 293 cells with a full-length $hP2X_4$ cDNA cloned in the mammalian expression vector pcDNA3 (InVitrogen, San Diego, CA) was carried out using the calcium phosphate precipitation method (28). Independent foci were selected and expanded in the continuous presence of geneticin (500 μg/ml; Sigma).

Measurements of fractional Ca^{2+} were performed according to a previously described method (29, 30). Briefly, HEK 293 cells stably transfected with $hP2X_4$ cDNA were plated onto circular coverslips and measured after 1–3 days. Whole-cell recordings and simultaneous Fura-2 measurements were made using an intracellular solution that contained 140 mM KCl, 10 mM HEPES, and 1 mM Fura-2, pH 7.2, and an external Ringer's solution containing 135 mM NaCl, 5.4 mM KCl, 1.8 mM $CaCl_2$, 1 mM $MgCl_2$, and 10 mM HEPES, pH 7.2. For fluorescence calibration experiments, the intracellular solution used contained 100 mM *N*-methyl-D-glucamine, 10 mM HEPES, and 1 mM Fura-2, pH 7.2, and the extracellular solution contained 100 mM *N*-methyl-D-glucamine, 10 mM HEPES, and 10 mM $CaCl_2$, pH 7.2. It is accepted that the use of 1 mM Fura-2 is sufficiently enough to capture all of the calcium entering the cell so that the fluorescence decrement at 390 nm is directly proportional to the Ca^{2+} influx (29). During recording, the cells were continuously perfused with the appropriate extracellular solution. The agonist was applied from a nearby glass pipette by pressure supplied through a peristaltic pump. ATP was first applied 4 min after onset of whole-cell recording, when sufficient equilibration of Fura-2 would have been reached. To compensate for variations in excitation light intensity, the fluorescence amplitude was normalized by using "standard beads" (diameter, 4.5 μm; Polyscience) measured on the same experimental day; 1 bead unit represents the average amplitude of the fluorescence signal at 390 nm (F_{390nm}) of five standard beads. Membrane currents were recorded using a computer-based EPC-9 amplifier and Pulse software. Currents were low-pass filtered at 3 kHz.

Results

Structure and tissue distribution of the human $P2X_4$ receptor. Using degenerate oligonucleotides for conservative P2X sequences and human brain cDNA, we isolated an amplification fragment (~750 bp) that showed a high sequence homology with previously identified P2X receptors. Using this PCR fragment, we screened under low-stringency conditions a human cDNA library derived from total brain mRNA. Eleven independent cDNA clones were isolated that strongly hybridized to the ^{32}P-labeled probe. Results from restriction endonuclease mapping, Southern blotting, transcription unit search, and DNA sequence analysis revealed that overlapping cDNAs had been identified rather than a full-length clone. A common *Sca*I site was used to ligate two overlapping clones, thereby completing a full-length cDNA. The open reading frame of the $hP2X_4$ is 1164 bp long, encoding a 388-amino acid polypeptide. A computer search of GeneBank using BLAST (GCG, Wisconsin Sequence Analysis Software, Genetics Computer Group, Madison, WI) revealed that the encoded protein shares significant sequence identity (87%) (Fig. 1) with that of the recently cloned $rP2X_4$ (15), suggesting that the cDNA we isolated is the correspondent human isoform ($hP2X_4$). The $hP2X_4$ protein has six consensus sites for *N*-glycosylation, N-X-(S/T), which are conserved in the rat receptor. Differences between the amino acid sequences of both species are mostly conservative substitutions, located within the putative extracellular loop. In addition, three hydrophobic changes are present in the second putative transmembrane segment (Fig. 1).

We examined $hP2X_4$ mRNA expression in multiple human tissues by amplifying (through RT-PCR) cDNA from brain, heart, spinal cord, adrenal gland, liver, kidney, and skeletal

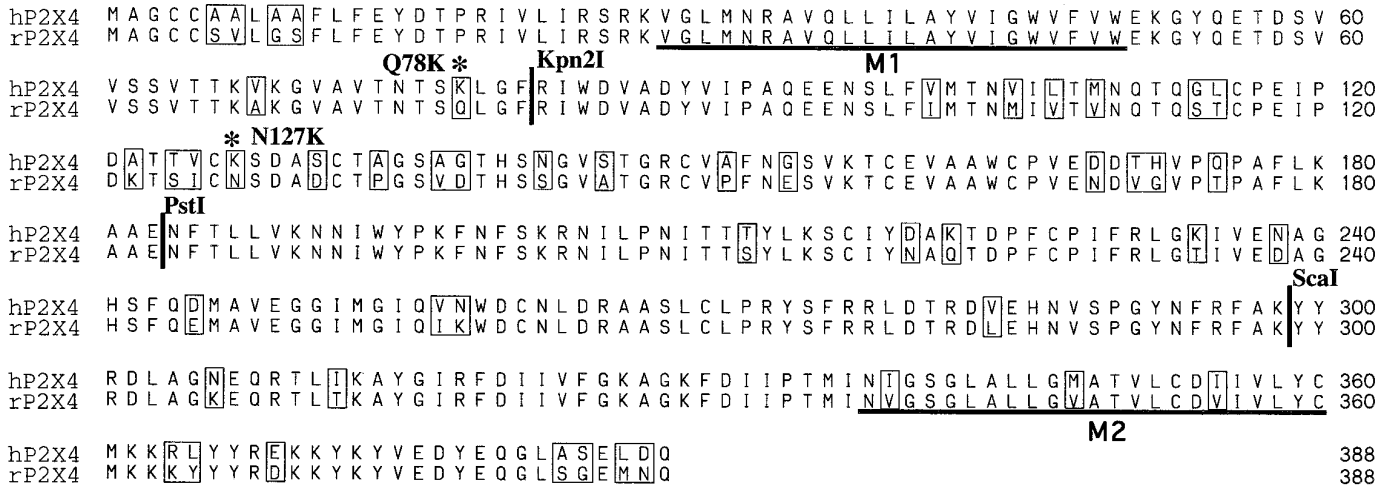

Fig. 1. Amino acid sequence alignment for the $hP2X_4$ and $rP2X_4$ receptors. *Open boxes*, nonconserved residues. *Circles*, *N*-glycosylation sites [consensus site N-X-(S/T)]. *Underlined*, proposed transmembrane segments. The approximate positions in the correspondent protein sequence for endonuclease restriction enzymes used to create chimeric human/rat constructs are indicated. *, Single-point mutations in the rat $P2X_4$ receptor, Q78K and N127K.

muscle. The $hP2X_4$ mRNA shows a broad expression pattern, being detected as a single amplification band in all tissues analyzed (Fig. 2). The signal specificity was confirmed by nucleotide sequencing. This finding is consistent with data observed for the rat $P2X_4$ (15), suggesting that in both species the $P2X_4$ mRNA distribution is very similar.

Chromosomal localization on the $hP2X_4$ gene on chromosome 12. A 1.7-kb cDNA encoding the $hP2X_4$ receptor was labeled with biotinylated-dATP by nick translation and hybridized to normal metaphase chromosomes derived from PHA-stimulated peripheral blood lymphocytes using FISH. Under the conditions used, the hybridization efficiency was ~87% for this probe (among 100 checked mitotic figures, 87 of them showed signals on one pair of the chromosomes) (Fig. 3a). The DAPI banding was used to identify the specific chromosome; the assignment between signal from probe and the long arm of chromosome 12 could be obtained (Fig. 3b). There was no additional locus detected by FISH under these experimental conditions. Therefore, the $hP2X_4$ gene is located at human chromosome 12, region q24.32 (Fig. 3c).

Functional expression of $hP2X_4$ yields ATP-activated homomeric channels. To characterize the functional and pharmacological properties of $hP2X_4$, we expressed the receptor in *X. laevis* oocytes. In cRNA-injected oocytes, ATP evoked a rapid inwardly rectifying current that slowly desensitized in the continuous presence of the agonist (Fig. 4, a and b). Noninjected oocytes routinely failed to respond to ATP. The rank order of agonist efficacy for different nucleotide analogs (100 μM) follows a pattern similar to that of the rat receptor: ATP $\gg$ 2MeSATP $\geq$ CTP $>$ α,β-meATP $>$ dATP. For $rP2X_4$ (15), we found the agonist 2MeSATP to be much less effective than ATP. Representative currents elicited by the various agonists are shown in Fig. 4a. No significant responses ($<$1% of ATP current) were detected with 100 μM of ADP, AMP, β,γ-meATP, GTP, and adenosine or with the neurotransmitter receptor agonists acetylcholine (with 100 μM atropine), nicotine, glutamate, γ-aminobutyric acid, glycine, and 5-hydroxytryptamine$_3$ (all at 100 μM). Construction of a dose-response curve to ATP (Fig. 4c) revealed that the EC_{50} value was 7.4 $\pm$ 0.5 μM ATP and the Hill coefficient, n_H, was 1.4 $\pm$ 0.1 (five determinations). These values are virtually identical to the value previously reported for $rP2X_4$ (15). Partial agonist dose-response curves for CTP and 2MeSATP are also shown in Fig. 4c.

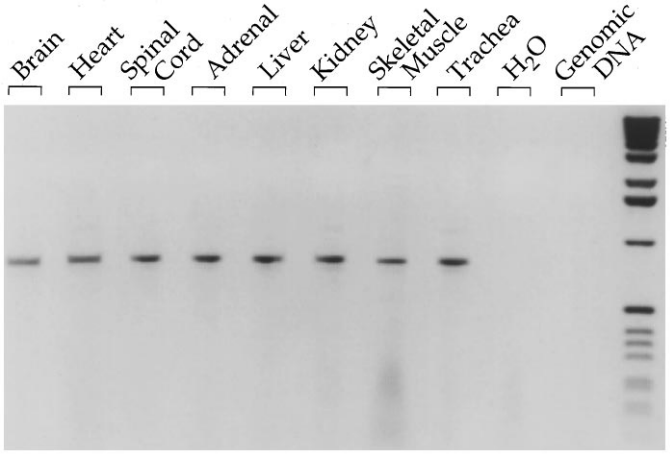

Fig. 2. Tissue distribution of $hP2X_4$ mRNA determined by RT-PCR in a color-inverted video image of the DNA bands stained with ethidium bromide. cDNAs from various human tissues were analyzed by PCR using specific oligonucleotides for the $hP2X_4$ gene, and the amplification products were separated in a 1% agarose gel. A single band of the predicted size was detected (792 bp) in every tissue. Samples using human genomic DNA (0.5 μg) and no DNA (H_2O) were performed as negative controls. *Size markers*, 1-kb ladder (GIBCO).

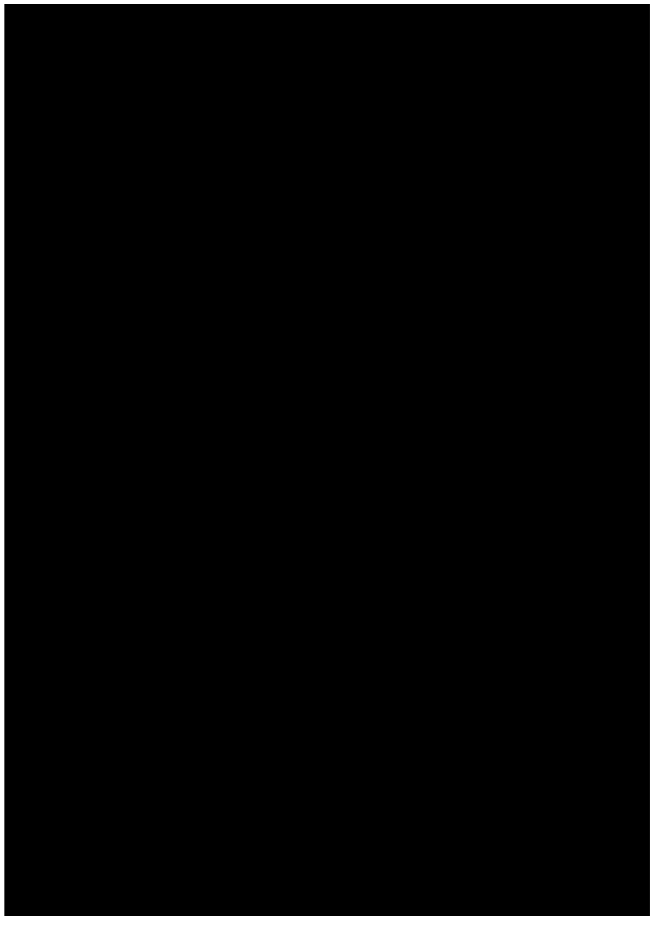

Fig. 3. FISH analysis of human metaphase chromosomes using a biotinylated-human $P2X_4$ probe. a, Representative chromosome spread of PHA-stimulated human lymphocytes showing the localization of FISH signals (*arrow*). b, Same mitotic figure as in a stained with DAPI to identify the labeling of chromosome 12. c, Chromosome 12 denoting the localization of the $hP2X_4$ gene at 12q24.32.

Modulation by $[Zn^{2+}]_o$ of the $hP2X_4$. It has been reported that $[Zn^{2+}]_o$ increases the amplitude of ATP-activated currents through both native (31–33) and cloned ($P2X_2$ and $P2X_4$) P2X receptors. Coapplication of 5 μM ATP and 10 μM Zn^{2+} markedly increases the amplitude of the $hP2X_4$-evoked current (Fig. 5a). This modulation exhibits a bell-shaped dose-response dependence on the Zn^{2+} concentration (Fig. 5b). Maximal potentiation occurs at relatively low $[Zn^{2+}]_o$ in the range of 5–10 μM. A further rise of $[Zn^{2+}]_o$ ($>$100 μM) diminishes the relative potentiation, and at even higher concentrations (1 mM), a dramatic inhibition of the ATP-evoked response is observed. Both the potentiation and inhibition by $[Zn^{2+}]_o$ were fully reversed within $<$3 min of washout of the Zn^{2+} ions. To examine in more detail the $[Zn^{2+}]_o$ modulation of the $hP2X_4$ currents, we analyzed the agonist dose-response curve in the presence of 10 μM $[Zn^{2+}]_o$. In the presence of Zn^{2+}, the apparent affinity for ATP is increased (a ~3-fold

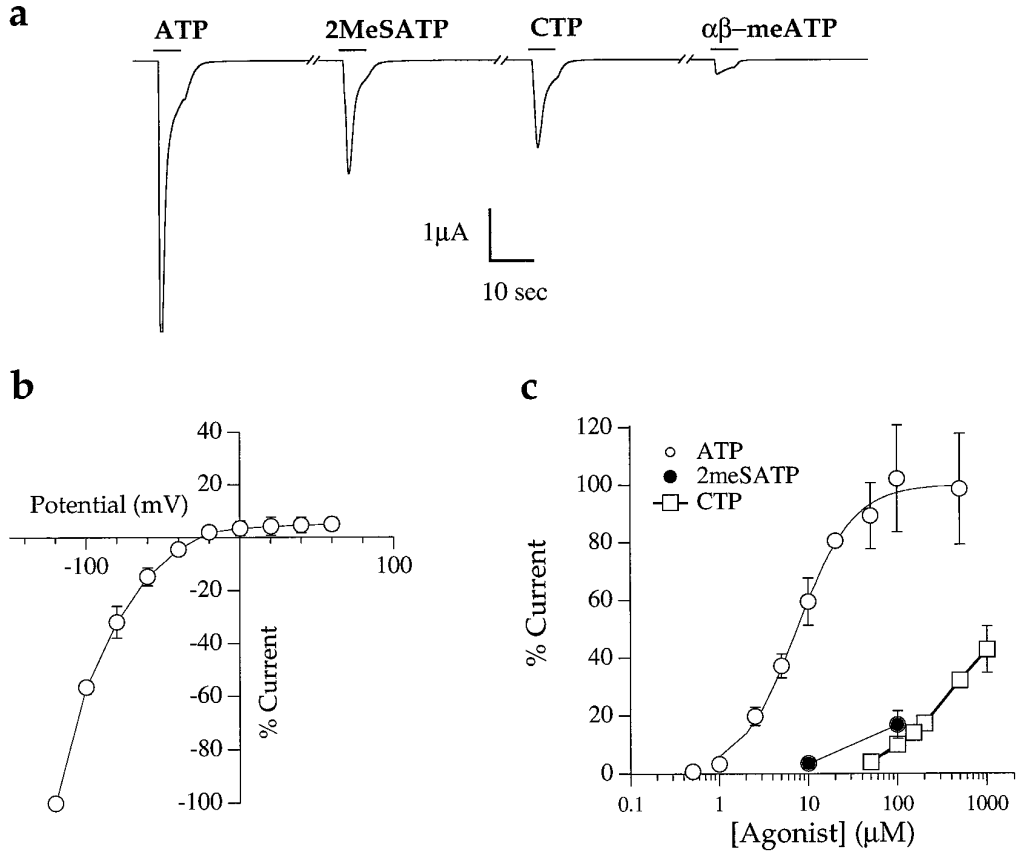

Fig. 4. Functional expression of recombinant $hP2X_4$ receptors in *X. laevis* oocytes. a, Representative inward currents elicited by application (5 sec) of various P2X agonists (100 μM). Holding potential is −70 mV. b, Maximal currents elicited by 50 μM ATP at different holding voltages (normalized to the response at −120 mV, three determinations). c, Dose-response curves of $hP2X_4$ for ATP, 2MeSATP, and CTP (four determinations). *Continuous line for ATP*, fit to the data using the equation $I = I_{max}/[1 + (EC_{50}/L)^{nH}]$, where I is the actual current for a ligand concentration (L), n_H is the Hill coefficient, and I_{max} is the maximal current (EC_{50} = 7.44 ± 0.53, n_H = 1.38 ± 0.12). The amount of current obtained at each ATP concentration was normalized to the current obtained with 100 μM ATP. a and b, Mg^{2+} in the standard solution was replaced by Ca^{2+}. c, Standard Mg^{2+} solution was used.

reduction for EC_{50}) and the dose-response curve shifts to the left. However, the maximal response is not altered (Fig. 5c).

To determine whether $[Zn^{2+}]_o$ modulation involved binding to the channel pore structure, we examined whether there was any voltage dependence to the $[Zn^{2+}]_o$ action. In these experiments, the currents were recorded using voltage ramps that spanned −100 to +70 mV in 150 msec. Currents were first measured in the presence of ATP alone and then in the presence of varying $[Zn^{2+}]_o$. The current ratio was calculated by dividing the latter by the former. Fig. 5d plots the current ratio in the presence of 5 and 500 μM $[Zn^{2+}]_o$. If Zn^{2+} binds to the ion pore, one would expect the current ratio to change over a certain voltage range. This was not the case, demonstrating that Zn^{2+} does not directly interact with the pore of $P2X_4$. Similar results were obtained when voltage step pulses of 2-sec duration were applied instead of voltage ramps (data not shown).

The homomeric $hP2X_4$ channel has a high Ca^{2+} permeability. The $hP2X_4$ receptor, like the other characterized recombinant P2X receptors, is equally permeable to the monovalent ions Na^+ and K^+, whereas it is not permeable to the anion Cl^- (data not shown). It has been demonstrated that some native and recombinant P2X receptors, including the $rP2X_4$, conduct Ca^{2+} with high permeability for this divalent cation (5, 14, 15, 34). To determine the relative contribution of Ca^{2+} to the total current through recombinant $hP2X_4$ channels, we performed simultaneous measurements of membrane current using whole-cell patch-clamp techniques and intracellular Ca^{2+} using the fluorescence indicator Fura-2. The calibration of the receptor-dependent Ca^{2+} influx in physiological solutions was related to pure Ca^{2+} signals through the same receptors when Ca^{2+} was the only charge carrier (calibration solution) (34). After the application of 50 μM ATP to HEK 293 cells expressing recombinant $hP2X_4$ receptors, we calculated the ratio (F/Q) of the fluorescence decrement (ΔF_{390nm}) to the total charge (Q_{hP2X_4}) when both calibration and Ringer's solutions were used. A typical recording of ΔF_{390nm} and voltage-clamped ATP-induced currents in test solutions is shown in Fig. 6. By dividing the F/Q ratio obtained in the Ringer's solution by the F/Q ratio in calibration solution, in which the entire ATP-activated current is expected to be carried exclusively by Ca^{2+}, the fractional Ca^{2+} current (30) was calculated to be 8. 24 ± 0.36% (five determinations).

The $hP2X_4$ receptor shows a much higher sensitivity to P2X antagonists than the $rP2X_4$ receptor. The most unexpected pharmacological properties of the rat $P2X_4$ receptor are the low sensitivities to the antagonists suramin and PPADS (15). Indeed, sensitivity to suramin has been used to define P2X-mediated currents in native systems. Only in rat submandibular gland has it been reported that suramin is a weak antagonist for ATP-induced currents (18). The human $P2X_4$ receptor had a low sensitivity for suramin compared with other P2X receptors (Fig. 7a) (IC_{50} = 178.1 ± 46.9; four determinations), but the antagonist effect was clearly more potent than that for the rat counterpart ($IC_{50} > 500$ μM, 5 μM ATP) (15). Prolonged exposure to 100 μM suramin (for 15 min before ATP application) did not reveal any variation in the antagonist efficacy (data not shown). The suramin block was reversed completely after a 3-min perfusion with extracellular solution.

The most remarkable pharmacological difference between

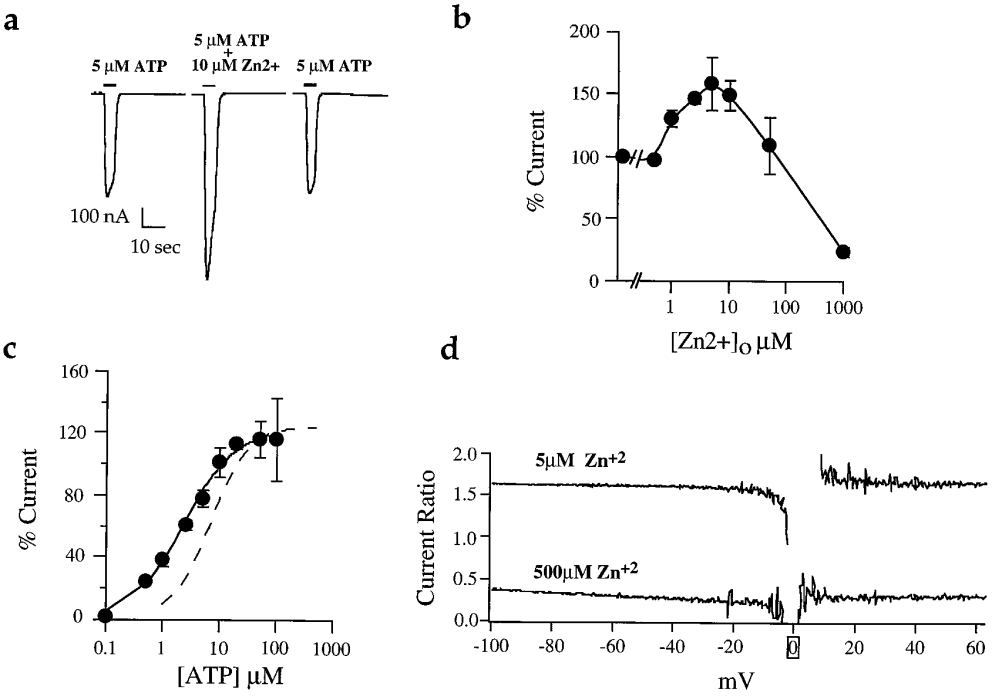

Fig. 5. Modulation by $[Zn^{2+}]_o$ of hP2X$_4$ ATP-elicited currents. a, Recordings of current activated by 5 μM ATP in the presence or absence of 10 μM Zn^{2+}. Recordings were obtained sequentially from the same oocyte, with a 3-min wash-out between applications. b, Relative enhancement or impairment of maximal ATP elicited currents (compared with control with 5 μM ATP alone) plotted as a function of $[Zn^{2+}]_o$ (four determinations). Note the dual effect of Zn^{2+}, potentiation at low concentrations (<10 μM), and block at higher concentration (>100 μM). c, Dose-response curve for ATP in the presence of 10 μM Zn^{2+}. Data were fitted to the equation described in the legend to Fig. 4c (*continuous line*), giving an EC_{50} value of 2.39 ± 0.26 with an n_H value of 0.99 ± 0.09 (three determinations). For comparison, the fit to the dose-response curve for ATP alone (data from Fig. 4c) is shown (*dashed line*). The amount of current obtained for each data point was normalized to the current obtained in the presence of 5 μM ATP, in the presence (*continuous line*) or absence (*dashed line*) of 10 μM Zn^{2+}, respectively. d, Current ratios obtained under voltage ramps (−100 to +70 mV in 150 msec) in the presence or absence of $[Zn^{2+}]_o$, I(presence)/I(absence). All recordings were obtained in standard Mg^{2+} solution at a holding potential of −70 mV.

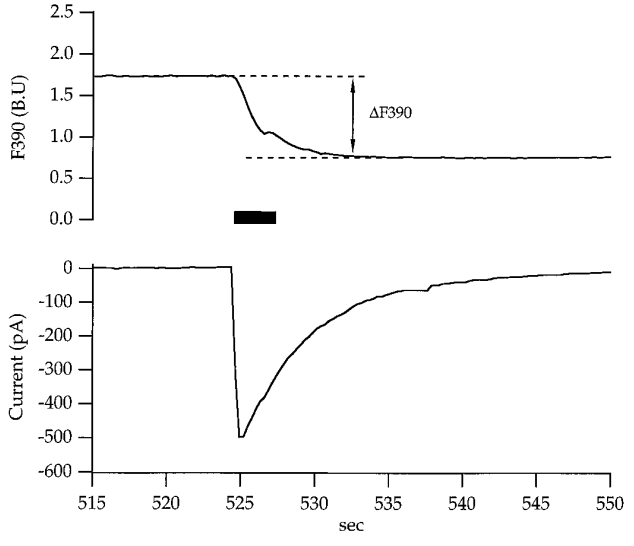

Fig. 6. Ca^{2+} influx through hP2X$_4$ receptors. Simultaneous (*bottom*) recordings of hP2X$_4$ receptor currents and (F_{390nm}, *top*) Fura-2 fluorescence at 390 nm were made from hP2X$_4$-transfected HEK 293 cells. The cell was continuously perfused with the test solution and voltage-clamped at −70 mV. *Solid bar above the current trace*, application of the agonist (ATP, 50 μM). The decrement of F_{390nm} (ΔF_{390nm}) caused by the rise of intracellular Ca^{2+} is indicated.

the hP2X$_4$ and the rP2X$_4$ receptors concerns the PPADS antagonist efficiency. The rP2X$_4$ receptor has been shown to be insensitive to PPADS block even at concentrations as high as 500 μM (15, 18). However, the same drug was an effective antagonist of the human isoform (IC_{50} = 27.5 ± 3.4; five determinations) (Fig. 7a) when the blocker was incubated for 8 min before agonist stimulation. The recovery of the current, after PPADS block, was complete within the 3-min wash period used between two consecutive agonist applications.

Other general P2 antagonists, such as bromphenol blue and the two isomers of reactive blue (basilen blue and cibacron blue), also proved to be effective blockers. When we compared the rP2X$_4$ with hP2X$_4$ receptors, cibacron blue as well as bromphenol blue were clearly more potent at the human receptor (Fig. 7b and Table 1). No differences were observed for basilen blue (Table 1). Similar to the PPADS and suramin block, the maximal current fully recovered after 3 min of wash-out.

Specific protein domains determine the different pharmacology for antagonists. The important pharmacological differences between these very homologous proteins prompted us to investigate the structural determinants that confer the distinct antagonist phenotypes. Several chimeric receptors between the rP2X$_4$ and hP2X$_4$ receptors were made and then expressed in *X. laevis* oocytes. All of the constructions resulted in functional ATP-activated channels, with wild-type kinetics of activation and desensitization (not shown). We characterized the antagonist sensitivities of these chimeric proteins by using concentrations of suramin (200 μM) or PPADS (100 μM) that permitted us to differentiate between the rat and human phenotypes. Every chimeric

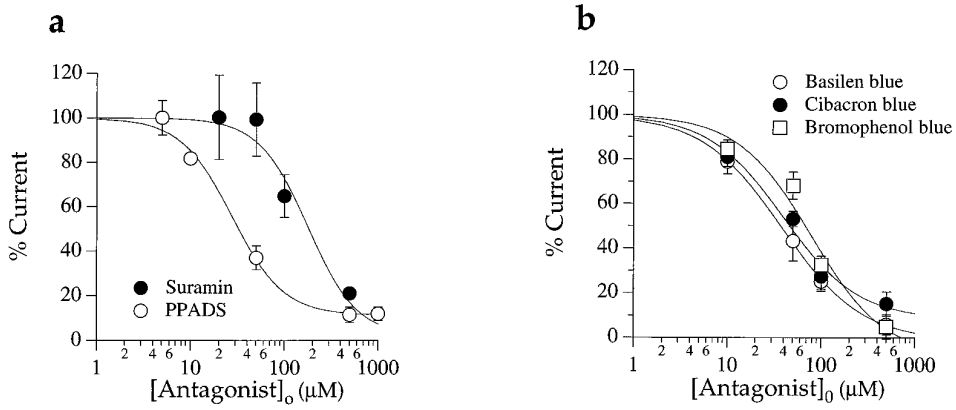

Fig. 7. Inhibition of $hP2X_4$ receptor currents by different antagonists. a, Relative maximal currents (5 μM ATP) obtained in the presence of increasing concentrations of suramin or PPADS. *Continuous lines*, fits to the data as described in the legend to Fig. 4c. Suramin (IC_{50} = 178 ± 46.9 μM; four determinations) was coapplied with the agonist. Prolonged exposure (≤15 min) did not affect the blocking efficiency. PPADS (IC_{50} = 27.5 ± 3.4 μM; five determinations) was preincubated for 8 min, and subsequently the agonist was applied. For PPADS concentrations of <50 μM, the agonist was coapplied with the appropriate PPADS concentration studied. The recordings were carried out in the standard Mg^{2+} solution at a holding potential of −70 mV. b, $hP2X_4$ receptor block by using cibacron blue, basilen blue, and bromphenol blue. The maximal relative currents (5 μM ATP) obtained on coapplication of the antagonist and ATP are plotted with the fit to the data (*continuous line*) as described in the legend to Fig. 4c. The calculated IC_{50} values are basilen blue, 38 ± 2.1 μM; cibacron blue, 39 ± 10.9 μM; and bromphenol blue, 78 ± 4.7 μM (more than three determinations). Data were obtained in standard Mg^{2+} solution at a holding potential of −70 mV.

TABLE 1

Antagonist IC_{50} values

The $rP2X_4$ and the $P2X_4$ receptors exhibit different antagonist affinities when homomeric receptors are expressed in *X. laevis* oocytes. IC_{50} values (mean ± standard deviation) were calculated from the fit of the equation described in the legend to Fig. 4c to the data (5 μM ATP). The low sensitivity of $rP2X_4$ receptor for suramin and PPADS disallowed the estimation of the IC_{50} values. The number of experiments are indicated in parentheses.

	IC_{50}	
	$hP_{2\times4}$	$rP_{2\times4}$
Suramin	178.1 ± 46.9 (4)	>500 (3)
PPADS	27.5 ± 3.4 (5)	>500 (3)
Bromphenol blue	78.3 ± 4.7 (3)	301.5 ± 67.7 (3)
Basilen blue	38.1 ± 2.1 (4)	46.2 ± 9.2 (3)
Cibacron blue	39.2 ± 10.9 (4)	128.3 ± 11.8 (5)

receptor containing $hP2X_4$ sequences in the domain bracketed by the restriction enzymes *Kpn*2I and *Pst*I (Fig. 1) demonstrated a human wild-type PPADS sensitivity. Furthermore, all of the constructs compassing a rat *Kpn*2I/*Pst*I sequence were inefficiently blocked by the same drug, thereby resembling the rat receptor (Fig. 8). Therefore, molecular determinants located on the *Kpn*2I/*Pst*I domain determine a higher PPADS sensitivity for the $hP2X_4$ receptor.

Based on a previous report (18) that demonstrated a role for a specific lysine amino acid in determining the PPADS blocking efficiency, we investigated the role of lysine residues on PPADS binding. Despite the existence of many amino acid variations through the rat and human *Kpn*2I/*Pst*I domain, only one lysine residue is exclusively present in the human sequence, K127 (Fig. 1). Single-point mutation of $rP2X_4$ (N127K) did not confer sensitivity for PPADS block (Fig. 8).

Interestingly, when we assayed the suramin sensitivity of the different constructs, a distinct region of the protein was found to be crucial for the antagonist blocking efficiency. Suramin was very effective in antagonizing ATP-evoked currents when the chimeric receptors contained the amino-terminal *Kpn*2I domain (Figs. 1 and Fig. 8). Indeed, a chimeric receptor comprising a human amino-terminal *Kpn*2I domain on the $rP2X_4$ receptor (human/rat *Kpn*2I) showed a very high suramin affinity, with an IC_{50} value of 13 ± 2 μM (six determinations), which is >50 and ~14 times more sensitive than the $rP2X_4$ and $hP2X_4$ wild-type receptors, respectively. A single-point mutation on the rat receptor Q78K was sufficient to account for the increase in suramin affinity (Fig. 8). The ATP binding affinity of this mutant, $rP2X_4$ (Q78K), was not affected (~8 μM; three determinations), suggesting that the amino acid substitution did not modify the overall structure of the receptor.

Discussion

We cloned the first P2X purinergic receptor from human brain, and it shows a high degree of homology with the described $rP2X_4$ (87% identity). The two receptors are equally long (388 amino acids) and differ mostly in the putative extracellular loop. Interestingly, three conservative changes are located in the second hydrophobic segment (M2 in Fig. 1), but complete identity is found in the first putative transmembrane segment (M1). Other important structural features, like *N*-glycosylation sites and proline or cysteine residues, are conserved.

Using hybridization of a $hP2X_4$ probe for FISH to normal metaphase chromosomes, the $hP2X_4$ has been located in chromosome 12, locus q24.32. The $hP2X_1$ receptor has been previously mapped to chromosome 17 p13.3 (11), and the $hP2X_3$ gene is located in the long arm of chromosome 11, locus q12 (35). These results reveal that every hP2X receptor gene that has been cloned maps to different chromosomes. A data base search for genetically linked human diseases did not reveal any known pathology that could be related with the $hP2X_4$ gene.

The pattern of $hP2X_4$ mRNA expression in human tissues observed by RT-PCR parallels the distribution previously found for the rat homologue receptor (15). We found expression in every tissue studied, including skeletal muscle. Although extracellular ATP activates contraction in vascular and visceral smooth muscle cells as well as in cardiomyocytes (1), fast ATP-activated currents have not been reported in

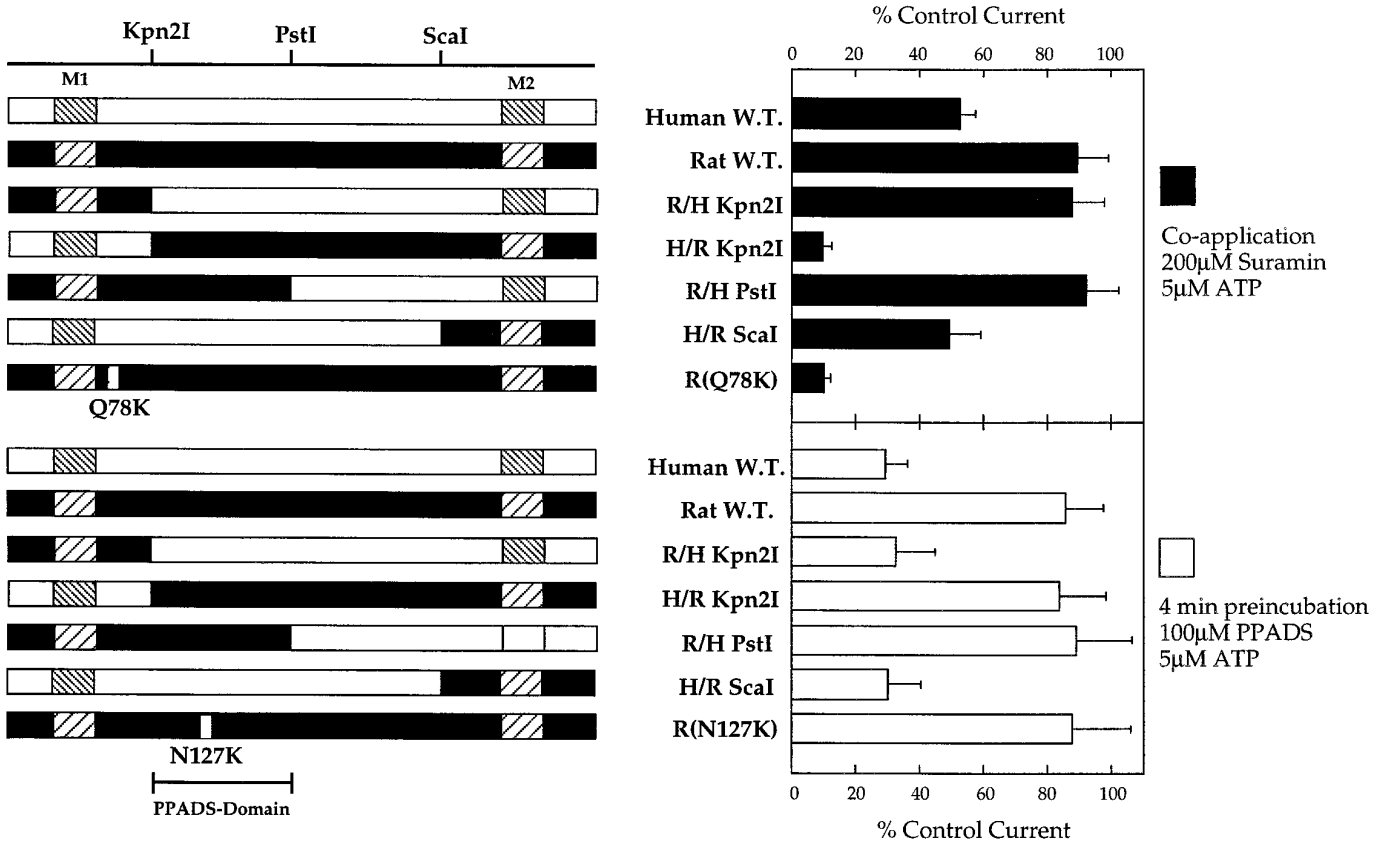

Fig. 8. Specific domains determine the PPADS and suramin blocking differences between the $hP2X_4$ and $rP2X_4$ receptors. *Left*, analyzed constructions[black ($rP2X_4$) or white ($hP2X_4$) sequences, respectively]. The approximate positions for the endonuclease restriction enzymes used are indicated, as well as the single-point mutations on the $rP2X_4$ receptor. *Right*, *bars*, percentage current obtained on coapplication of 200 μM suramin and the agonist (*solid bars*) or after 4-min preincubation of 100 μM PPADS (*open bars*) after agonist stimulation (5 μM ATP). The currents were normalized to the control response (100%) obtained on the application of the agonist in the absence of the blocker (six or more determinations). Data were obtained in standard Mg^{2+} solution at a holding potential of -70 mV.

adult skeletal muscle cells. However, ATP-gated ion channels have been extensively characterized in chick embryonic myoblast and myotubes (1). Unfortunately, the functional presence of P2X receptors in human skeletal muscle has not been studied, and the high sensitivity of the RT-PCR technique used in this report does not allow us to discriminate between a certain expression of transcripts in skeletal muscle cells and expression in the vascular system supplying this organ.

The $hP2X_4$ protein conforms functional homomeric ATP-activated channels when expressed in heterologous cellular systems. The agonist-induced currents recorded from *X. laevis* oocytes injected with $hP2X_4$ cRNA show a very similar agonist profile to that reported for the rat isoform (15). Thus, the $hP2X_4$ receptor exhibits a low apparent ATP affinity ($\sim$8 μM) and no sensitivity to α,β-meATP ($EC_{50} \gg 100$ μM). Nevertheless, ATP is a more powerful agonist than 2MeSATP for the $hP2X_4$, which in agreement with our published data for the rat isoform expressed in *X. laevis* oocytes (15) and in contrast with another report that described the same potency for both agonists when the rat receptor was expressed in HEK 293 cells (18).

Chelatable zinc is present in presynaptic vesicles of central excitatory neurons, most notably in the hippocampal hilus, CA1, and the mossy fibers (36). $P2X_4$ transcripts occur in many regions of the central nervous system (15), including all areas of the hippocampus where high density of synaptically released Zn^{2+} has been detected (36). We report here that the $hP2X_4$ receptor is modulated by $[Zn^{2+}]_o$ in a non-voltage-dependent manner. The allosteric modulation of the $P2X_4$ channel by $[Zn^{2+}]_o$ nicely mirrors the behavior of the ATP-activated currents in dissociated neurons from both rat nodose ganglia (31) and rat superior cervical ganglia (32, 33). The expression of the $rP2X_4$ receptor in these specific neurons (16) suggests that this protein could participate as a subunit of the native P2X receptor, thereby conferring $[Zn^{2+}]_o$ sensitivity. Because of the low concentration of Zn^{2+} required to modulate $P2X_4$ gating, it is reasonable to propose that vesicular release of Zn^{2+} into the synaptic cleft might be a physiological mechanism of regulating $P2X_4$ channel activity. Interestingly, it was recently reported that after transient forebrain ischemia in rats, $[Zn^{2+}]_o$ enters the cells through undetermined channels and accumulates specifically in degenerating neurons in the hippocampal hilus and CA1 (37). The fact that many cells in hypoxia release ATP into the extracellular media raises the intriguing possibility that $P2X_4$ might be involved in Zn^{2+}-induced neuronal death. Nevertheless, the putative Zn^{2+} permeation through P2X receptors has not been addressed.

Although the relative Ca^{2+} permeability to monovalent cations of some recombinant P2X receptors, including $rP2X_4$, has been previously demonstrated from reversal potential measurements (15), the actual amount of Ca^{2+} influx is still

not known. Using a combination of whole-cell patch-clamp and Fura-2 fluorescence measurements in HEK cells transfected with $hP2X_4$, we determined that the recombinant $hP2X_4$ channel permeates a substantial amount of Ca^{2+} ions under physiological ionic conditions. The percentage of current carried by Ca^{2+} is ~8%, a value very close to that previously reported for native ATP currents in sympathetic neurons from rat superior cervical ganglia (34). Among the ligand-gated channels, a higher Ca^{2+} fractional current (8–14%) has been reported only for some subunit combinations of *N*-methyl-D-aspartate-type glutamate receptors (see Ref. 30 and references therein). The high Ca^{2+} permeation through $hP2X_4$ receptors suggests that activation of these proteins may directly underlie activity-dependent Ca^{2+} signals while contributing to synaptic transmission (38).

The most remarkable difference between the $rP2X_4$ and $hP2X_4$ receptors concerns the antagonist sensitivities. The compounds suramin and PPADS block the $hP2X_4$ with much higher efficiency than $rP2X_4$ (Table 1), indicating the existence of specific structural determinants controlling the binding for these purinergic antagonists. We identified a domain of ~100 amino acids (81–183) located in the large extracellular loop of the receptor that account for the higher PPADS sensitivity in the human isoform. In the primary sequence, this region is upstream of amino acid 249 (for $P2X_4$), a position that requires a lysine residue to confer a high and irreversible PPADS sensitivity in the $rP2X_4$ receptor (18). Therefore, like other ligand-gated channels, a multivalency binding site that involves domains distant in the primary structure is probably essential for PPADS/receptor interactions. Among the 22 amino acids that differ within the PPADS-sensitive domain between the rat and human receptors, only one lysine residue is found exclusively in the human sequence (K127) but not in the rat homologue (N127). Mutation of the $rP2X_4$ receptor N127K did not generate the human phenotype, suggesting that this residue does not contribute to the chemical binding of PPADS.

A detailed analysis of the different apparent affinities for suramin of the $rP2X_4$ and $hP2X_4$ receptors allowed us to identify a single residue that critically controls the blocking efficiency of this compound. Thus, the single-point mutation $rP2X_4$ (Q78K) enhances the suramin affinity by >50-fold. At physiological pH, suramin is negatively charged; consequently, we propose that electrostatic interactions could stabilize the chemical interaction between suramin and $P2X_4$ receptors. Protein sequence alignments of the $P2X_{1\text{-}6}$ receptors (10) show that this residue (amino acid 78 in $P2X_4$) is different in all cloned channels and that only the $hP2X_4$ receptor possesses a lysine in this position. Furthermore, the suramin-sensitive receptors $P2X_2$ and $P2X_3$ exhibit a protein deletion in this region, suggesting that different channels use different chemical mechanisms for suramin binding and block. A more detailed study is necessary to define the precise structural domains that delineate the binding sites of suramin and PPADS in the purinergic ligand-gated channels.

Acknowledgments

We are grateful to Katja Anttonen for excellent technical assistance, Barbara Scheulfer for expert cell culture assistance, and Dr. Anant Parekh for critically reading of and diligent correction of the manuscript. We acknowledge Dr. Henry Heng (SeeDNA Biotech, Downsview, Ontario, Canada) for FISH analysis.

References

1. Dubyak, G. R., and C. El-Moatassim. Signal transduction via P2-purinergic receptors for extracellular ATP and other nucleotides. *Am. J. Physiol.* **265:**C577–C606 (1993).
2. Surprenant, A., G. Buell, G., and R. A. North. P2X receptors bring new structure to ligand-gated ion channels. *Trends Neurosci.* **18:**224–229 (1995).
3. Chen, Z.-P., A. Levy, and S. L. Lightman. Nucleotides as extracellular signalling molecules. *J. Neuroendocrinol.* **7:**83–96 (1995).
4. Burnstock, G., and C. Kennedy. Is there a basis for distinguishing two types of P2-purinoceptors? *Gen. Pharmacol.* **16:**433–440 (1985).
5. Benham, C. D., and R. W. Tsien. A novel receptor-operated Ca^{2+} permeable channel activated by ATP in smooth muscle. *Nature (Lond.)* **328:**275–278 (1987).
6. Bean, B. P., C. A. Williams, and P. W. Ceelen. ATP-activated channels in rat and bullfrog sensory neurons: current-voltage relation and single-channel behaviour. *J. Neurosci.* **10:**11–19 (1990).
7. Abbracchio, M. P., and G. Burnstock. Purinoceptors: are there families of P2X and P2Y purinoceptors? *Pharmacol. Ther.* **64:**445–475 (1994).
8. North, R. A. Families of ion channels with two hydrophobic segments. *Curr. Opin. Cell Biol*. **8:**474–483 (1996).
9. Garcia-Guzman, M., F. Soto, B. Laube, and W. Stühmer. Molecular cloning and functional expression of a novel heart P2X receptor. *FEBS Lett.* **388:**123–127 (1996).
10. Soto, F., M. Garcia-Guzman, C. Karschin, and W. Stühmer. Cloning and tissue distribution of novel P2X receptor from rat brain. *Biochem. Biophys. Res. Commun.* **223:**456–460 (1996).
11. Valera, S., F. Talabot, R. J. Evans, A. Gos, S. E. Antonarakis, M. A. Morris, and G. N. Buell. Characterization and chromosomal localization of a human P2X receptor from the urinary bladder. *Recept. Channels* **3:**283–289 (1995).
12. Chen, C.-C., A. N. Akopian, L. Sivilotti, D. Colquhoun, G. Burnstock, and J. N. Wood. A P2X purinoceptor expressed by a subset of sensory neurons. *Nature (Lond.)* **377:**428–431 (1995).
13. Brake, A. J., M. J. Wagenbach, and D. Julius. New structural motif for ligand-gated ion channels defined by an ionotropic ATP receptor. *Nature (Lond.)* **371:**519–523 (1994).
14. Valera, S., N. Hussy, R. J. Evans, N. Adami, R. A. North, A. Surprenant, and G. Buell. A new class of ligand-gated ion channel defined by P2X receptor for extracellular ATP. *Nature (Lond.)* **371:**516–519 (1994).
15. Soto, F., M. Garcia-Guzman, J. M. Gomez-Hernandez, M. Hollmann, C. Karschin, and W. Stühmer. $P2X_4$: an ATP-activated ionotropic receptor cloned from rat brain. *Proc. Natl. Acad. Sci. USA* **93:**3684–3688 (1996).
16. Collo, G., R. A. North, E. Kawashima, E. Merlo-Pich, S. Neidhart, A. Surprenant, and G. Buell. Cloning of P2X5 and P2X6 receptors and the distribution and properties of an extended family of ATP-gated ion channels. *J. Neurosci.* **16:**2495–2507 (1996).
17. Evans, R. J., C. Lewis, G. Buell, S. Valera, R. A. North, and A. Surprenant. Pharmacological characterization of heterologously expressed ATP-gated cation channels (P2X purinoceptors). *Mol. Pharmacol.* **48:**178–183 (1995).
18. Buell, G., C. Lewis, G. Collo, R. A. North, and A. Surprenant. An antagonist-insensitive P2X receptor expressed in epithelia and brain. *EMBO J.* **15:**55–62 (1996).
19. Krug, M. S., and S. L. Berger. First strand cDNA synthesis primed with oligo(dT). *Methods Enzymol.* **152:**316–325 (1987).
20. Sanger, F., S. Nicklen, and A. R. Coulson. DNA sequencing with chain-termination inhibitors. *Proc. Natl. Acad. Sci. USA* **74:**5463–5468 (1977).
21. Sambrook, J., E. F. Fritsch, and T. Maniatis. *Molecular Cloning: A Laboratory Manual*. Cold Spring Harbor Laboratory Press, Cold Spring Harbor, NY (1989).
22. Li, Q., and G. Wu. A versatile and simplified non-random strategy for nucleotide sequencing. *Gene* **56:**245–252 (1987).
23. Heng, H. H. Q., J. Squire, and L. C. Tsui. High resolution mapping of mammalian genes by in situ hybridization to free chromatin. *Proc. Natl. Acad. Sci. USA* **89:**9509–9513 (1992).
24. Heng, H. H. Q., and L. C. Sui. FISH detection on DAPI banded chromosomes, in *Methods in Molecular Biology: In Situ Hybridization Protocols* (K. H. A. Cho, ed.). Humana Press, Clifton, NJ, 35–49 (1994).
25. R. M. Horton. In vitro recombination and mutagenesis of DNA, in *Methods in Molecular Biology* (B. A. White, ed.). Humana Press, Clifton, NJ, 251–261 (1993).
26. Melton, D. A. Translation of messenger RNA in injected frog oocytes. *Methods Enzymol.* **152:**288–296 (1987).
27. Stühmer, W. Electrophysiological recording from *Xenopus* oocytes. *Methods Enzymol.* **207:**319–345 (1992).
28. Chen, C., and H. Okoyama. High-efficiency transformation of mammalian cells by plasmid DNA. *Mol. Cell Biol.* **7:**2745–2752 (1987).
29. Burnashev, N., Z. Zhou, E. Neher, and B. Sakmann. Fractional calcium current through recombinant GluR channels of the NMDA, AMPA and kainate receptor subtypes. *J. Physiol.* **485:**403–418 (1995).

30. Neher, E. The use of fura-2 for estimating Ca^{2+} buffers and Ca^{2+} fluxes. *Neuropharmacology* **34:**1423–1442 (1995).
31. Li, C., R. W. Peoples, Z. Li, and F. F. Weight. Zn^{2+} potentiates excitatory action of ATP on mammalian neurons. *Proc. Natl. Acad. Sci. USA* **90:** 8264–8267 (1993).
32. Cloues, R., S. Jones, and D. A. Brown. Zn^{2+} potentiates ATP-activated currents in rat sympathetic neurons. *Pflueg. Arch. Eur. J. Physiol.* **424:** 152–158 (1993).
33. Cloues, R. Properties of ATP-gated channels recorded from rat sympathetic neurons: voltage dependence and regulation by Zn^{2+} ions. *J. Neurophysiol.* **73:**312–319 (1995).
34. Rogers, M., and J. A. Dani. Comparison of quantitative calcium flux through NMDA, ATP and ACh receptor channels. *Biophys. J.* **68:**501–506 (1995).
35. Garcia-Guzman M., W. Stühmer and F. Soto. Molecular characterization and pharmacological properties of the human $P2X_3$ purinoceptor. *Mol. Brain Res.*, in press.
36. Charton, G., C. Rovira, Y. Ben-Ari, and V. Leviel. Spontaneous and evoked release of endogenous Zn^{2+} in the hippocampal mossy fiber zone of the rat in situ. *Exp. Brain Res.* **58:**202–205 (1985).
37. Koh, J. Y., S. W. Suh, Gwag, B. J., He, Y. Y., Hsu, C. Y., and D. W. Choi. The role of zinc in selective neuronal death after transient global cerebral ischemia. *Science (Washington D. C.)* **272:**1013–1016 (1996).
38. D. E. Clapham. Calcium signaling. *Cell* **80:**259–268 (1995).

Send reprint requests to: Florentina Soto, Ph.D., Max-Planck-Institute for Experimental Medicine, Hermann-Rein-Str. 3, D-37075 Göttingen, Germany. E-mail: soto@mail.mpiem.gwdg.de